



Original Articles

EphB1 promotes the differentiation and maturation of dendritic cells in non-small cell lung cancer



Yaohuan Xie ^{a,d,e,1}, Liyang Zhang ^{c,f,g,1}, Lujuan Wang ^{a,d,e}, Bo Chen ^{c,f,g}, Xiaoting Guo ^{a,d,e}, Yanyi Yang ^h, Wenhua Shi ^{a,d,e}, Anqi Chen ^{a,b}, Junqi Yi ^{a,b}, Jingqun Tang ^{a,b,**}, Juanjuan Xiang ^{a,d,e,*}

^a Hunan Key laboratory of Early Diagnosis and Precise Treatment of Lung Cancer, The Second Xiangya Hospital, Central South University, Changsha, Hunan, 410013, China

^b Department of Thoracic Surgery, The Second Xiangya Hospital, Central South University, Changsha, Hunan, 410013, China

^c Department of Neurosurgery, Xiangya Hospital, Central South University, Changsha, Hunan, China

^d Cancer Research Institute, School of Basic Medical Science, Central South University, Changsha, Hunan, China

^e NHC Key Laboratory of Carcinogenesis and the Key Laboratory of Carcinogenesis and Cancer Invasion of the Chinese Ministry of Education, Xiangya Hospital, Central South University, Changsha, Hunan, China

^f Hypothalamic-pituitary Research Center, Xiangya Hospital, Central South University, Changsha, Hunan, China

^g National Clinical Research Center for Geriatric Disorders, Xiangya Hospital, Central South University, Changsha, Hunan, China

^h Health Management Center, The Second Xiangya Hospital, Central South University, Changsha, 410011, China

ARTICLE INFO

ABSTRACT

Keywords:

EphB1
Dendritic cells
COX-2
Lung cancer

EphB1 is implicated in numerous physiological and pathological processes, including nervous system diseases, cardiovascular diseases and cancers. It binds to membrane-bound ligands and drives bidirectional signaling. EphB1, along with its ligand ehrinB, plays a pivotal role in activating immune cells. However, despite its presence in dendritic cells (DCs), EphB1's involvement in the differentiation and maturation of DCs in cancers remains inadequately understood. In this study, we found compromised differentiation and maturation of DCs in EphB1^{-/-} mice bearing lung adenocarcinoma syngeneic tumors. Our in vitro assays revealed that EphB1 phosphorylation induced DC differentiation and maturation. Cox-2, a key enzyme involved in the production of proinflammatory molecules, is implicated in DC differentiation induced by phosphorylated EphB1. Additionally, the study has identified lead compounds that specifically target EphB1 phosphorylation sites. Collectively, this research on EphB1 phosphorylation has provided valuable insights into the regulation of immune cell functionality and holds the potential for the development of innovative therapeutic strategies for a range of diseases.

1. Introduction

Ephrin receptors (Ephs) are the largest family of receptor tyrosine kinases (RTKs) and have been implicated in numerous physiological and pathological processes. These receptors bind to membrane-bound ligands, leading to bidirectional signaling [1]. Eph receptors elicit both *cis*- and *trans*-signaling, where *cis*-signaling occurs when Eph receptors and ligand ephrins are coexpressed within the same cell, while *trans*-signaling arises from interactions between adjacent cells [2–4]. Importantly, Eph *cis*-signaling is implicated in the inhibition of *trans*-signaling

and attenuation of the RTK pathway [4–6]. Functionally, Eph signaling serves as a repulsive signal counteracting cell adhesion during development, cell migration, nervous system injury repair, and maintenance of gap junctions [7]. Notably, EphB1 has an intriguing dual role in tumors, with both tumor-suppressing and tumor-promoting effects evident across distinct malignancies [8,9]. EphB1 has been found to be upregulated in lung cancer biopsies compared to noncancer controls [10]. In our previous study, we found the regulatory roles of *cis*- and *trans*-signaling in lung cancer stem cell enrichment postchemotherapy [3].

Recent research has highlighted the involvement of Eph receptors

* Corresponding author. Hunan Key laboratory of Early Diagnosis and Precise Treatment of Lung Cancer, the Second Xiangya Hospital, Central South University, Changsha, Hunan, 410013, China.

** Corresponding author. Department of thoracic surgery, the Second Xiangya Hospital, Central South University, Changsha, Hunan, 410013, China.

E-mail addresses: tangjq@csu.edu.cn (J. Tang), xiangjj@csu.edu.cn (J. Xiang).

¹ These authors contributed equally to this work.

<https://doi.org/10.1016/j.canlet.2023.216567>

Received 13 July 2023; Received in revised form 12 November 2023; Accepted 27 November 2023

Available online 7 December 2023

0304-3835/© 2023 The Authors. Published by Elsevier B.V. This is an open access article under the CC BY-NC-ND license (<http://creativecommons.org/licenses/by-nd/4.0/>).

and ephrin ligands within the immune cell milieu. Eph receptors are widely expressed in immune cells and play a multifaceted role in immune cell differentiation and activation. Eph receptors, such as EphA3 and EphA2, have been unveiled as tumor-associated antigens [11]. Dendritic cells (DCs) loaded with the EphA2 peptide induce immune responses and reduce tumor burden [12,13]. Notably, ephrin-A1, an Eph ligand, has shown the capability to activate DCs in a rat glioma model [14]. EphB1 expression has been reported on plasmacytoid DCs, neutrophil, and CD4⁺ and CD8⁺ T cells [15,16]. In vitro assays have demonstrated the activation of T cells upon stimulation by Ephrin B ligands [17]. However, intriguingly, studies have also reported the inhibitory effects of high concentrations of ephrinB1 and ephrinB2 on T-cell activation [18,19]. Although the roles of EphB/ephrinB interactions in T-cells have been explored, their impact on other immune cell populations, particularly DCs, has not been well-explored. DCs capture, process, and present antigens to T cells, initiating and modulating immune responses. They also provide costimulatory signals and cytokines that influence T-cell activation, differentiation, and effector functions. Further research on the specific effects of EphB/ephrinB interactions in DCs could enhance our understanding of their influence on immune responses. Furthermore, the conflicting roles of EphB1 in tumorigenesis may vary depending on the context, while the differentiation and activation of immune cells are crucial factors. Notably, despite their significance across diverse diseases, FDA-approved drugs targeting Eph receptors are conspicuously absent.

This study aims to unravel the potential influence of EphB1 on tumorigenesis and its association with immune cell maturation. Our findings reveal enhanced tumorigenesis and impaired DC differentiation in EphB1^{-/-} mice, underscoring the contribution of EphB1 to this process. Moreover, our investigation identifies EphB1 phosphorylation as a trigger for DC differentiation and maturation. Our work extends to the identification of lead compounds targeting specific phosphorylation sites within EphB1 (602–896) that effectively enhance cancer immunity. Through these findings, we shed light on the intricate mechanisms by which EphB1-ephrinB2 interactions regulate DC biology and provide potential avenues for modulating immune responses in cancer.

2. Materials and methods

2.1. Cell culture

Murine Lewis lung cancer cells (LLCs) were cultured in DMEM/F12 medium (Procell #PM150312, China) with 10 % fetal bovine serum (FBS, Corning #35-081-CV, USA) in a humidified 5 % CO₂ incubator at 37 °C.

To obtain bone marrow cells from mice, tibias and femurs were flushed and pressed through a 70 µm strainer. After lysing the red blood cells with red blood cell lysis buffer, the cells were resuspended in complete RPMI 1640 medium, RPMI containing 10 % FBS(Corning, #35-081-CV), 1 mM Sodium Pyruvate (Procell # PB180422), 2 mM L-glutamine (Procell #PB180420), and 0.05 mM β-Mercaptoethanol (Procell #) and counted. All bone marrow cells were cultured in complete RPMI supplemented with 20 ng/mL GM-CSF (Peprotech #315-03-20, USA) and 10 ng/mL IL-4 (Peprotech #214-14-20). Every other day, half of the cell culture medium was renewed, and appropriate cytokines were added again. On Day 5, bone marrow-derived dendritic cells (BMDCs) were harvested using CD11c microbeads (Miltenyi Biotec #130-125-835, USA). If cell maturity needed to be detected, the cells were stimulated with 100 ng/mL LPS (Sigma Adrich #L2880, USA). When involved in differentiation, drugs were added to GM-CSF and IL-4 on Day 0.

2.2. Sample acquisition and patient-derived cell (PDC) generation

The patients coded “BM101” and “BM104” from the XYNS cohort were independently diagnosed and confirmed by two pathologists.

Primary lung nodules and brain metastases were confirmed through tumor histology and immunohistochemistry (IHC) staining. BM101 was found to have an EGFR mutation (EGFR-L858R), while BM104 was characterized as an ALK mutant (EML4-ALK rearrangement). In the case of BM101, the patient was initially diagnosed with an upper right lung mass and underwent radical tumor resection. The histopathological diagnosis was lung adenocarcinoma. Two months later, the patient had a headache, and magnetic resonance imaging (MRI) showed left cerebellum metastasis. Single brain metastases were resected, followed by stereotactic radiosurgery (SRS) of the tumor cavity. For BM104, the patient was initially diagnosed with left lung adenocarcinoma through a fine needle biopsy, and the IHC staining showed EML4-ALK positivity. Crizotinib was prescribed, but a subsequent brain MRI screening found a right occipital brain metastasis. SRS was used to treat the brain metastases, but the brain metastases was enlarged after 6 months. The brain metastases were subsequently removed under a microscope.

Fresh surgical tissues of NSCLC brain metastases were collected from the Department of Neurosurgery, Xiangya Hospital. The surgical tumor tissues were maintained and transferred to PBS and then mechanically dissociated and trypsinized using AccutaseTM (Stemcell Technologies), as previously described [20]. Briefly, after depleting erythrocytes, the resuspension was gently centrifuged at 1000 rpm/min for 10 min, and the pelleted cells were resuspended and maintained in Neurocult NSA Basal Medium and Proliferation Supplement (Stemcell Technologies # 05751, CAN), with 20 ng/mL EGF (Life Technologies # PHG0314, USA), and basic 20 ng/mL FGF (Peprotech #100-19). The NSCLC patient-derived cells (PDCs) used in this study were confirmed by serial passaging for more than five passages and fingerprinting with patient and patient-derived xenografts using short tandem repeats. All cell lines were confirmed to be free of mycoplasma. This study was approved by Central South University. (Animal ethics approval number: 2023030607). The work involving clinical tumor specimens and cells was approved by the Medical Ethics Committee of the Xiangya Hospital of Central South University (No. 202012388 & No. 2017121019) and informed consent was obtained in all cases.

2.3. Animal

EphB1-deficient mice (EphB1^{-/-}) were generated on a C57BL/6 background using a targeting vector that disrupted the third exon of mouse EphB1 genes was introduced. Animal experiments were conducted with protocols approved by Central South University, China. Six-week-old wild-type C57BL/6 mice and EphB1^{-/-} mice were randomly divided into 2 groups. Genomic DNA was extracted from tail biopsies of WT and KO mice using a standard DNA extraction protocol. Genotyping was performed using polymerase chain reaction (PCR) targeting the gene of interest. Primers were as follows that targeting regions flanking the knockout insertion site.

Forward Primer F1: 5'-CTATGTGTCTCCTTTGTAGCCC -3'

Reverse Primer R1: 5'-CTGAGGAATGCCAAAGAGGGTG -3'

The targeted allele is 647 bp long. PCR was carried out in a 25-µL volume for 35 cycles.

For the subcutaneous tumor model, LLCs were subcutaneously injected into syngeneic C57BL/6 mice. A mixture of 1×10^6 LLC in 100 µL of PBS and 100 µL of Matrigel Matrix (Corning) was injected into the flank of either WT mice or EphB1 knockout mice. In some experiments, mice were treated with intraperitoneal injections of 100 µL TNP-000386 (TOPSCIENCE #T7294, China) at a final concentration of 50 mg/kg every day for a week when the tumor size reached 75–100 cm³. Tumor growth was monitored daily by measuring tumor size and volume, which was calculated using formula V = (length × width²) / 2. Once the tumor volume reached 1500 mm³, the mice were euthanized.

For intracranial xenografts, BM101 and BM104 cells were harvested by trypsinization, resuspended in DMEM at a concentration of 1×10^5 tumor cells, and delivered intracranially at 5 µL/mouse. After 40 days, central nervous system anatomy and perfusion fixation were performed

to harvest mouse brains. Serum was isolated from each mouse before dissection.

2.4. Magnetic resonance imaging

In this study, magnetic resonance imaging was performed to measure intracranial tumor formation on a Siemens Prisma 3T, NUMARIS/4 syngo MR E11 4VE11C 8 channel mouse coil. Mice were imaged under isoflurane anesthesia (3 % to initiate anesthesia, 2.5 % for maintenance). A heating pad was used to maintain a constant body temperature throughout the imaging procedure. T2-Weighted Turbo Spin Echo sequences were also acquired with repetition and echo times of 2500 ms/65 ms. A 60-mm field of view and 256 x 256 matrix produced an image resolution of 0.2 mm × 0.2 mm × 1.5 mm with 11 matching axial slices.

2.5. Flow cytometry

The antibodies used for immunostaining were obtained from the following sources: CD11c (Proteintech #17342-1-AP, USA), EphB1 (Santa #5F10A4, USA) and EphB1 (phospho-Tyr594) (Biorbvt #orb187803, UK). The antibodies used for flow cytometry were as follows: CD45-APC-Cy7 (1:100 dilution, Biolegend #103116, USA), CD3-FITC (1:100 dilution, Invitrogen #MA5-16623, USA), CD4-PerCp/Cy5.5 (1:100 dilution, Biolegend #100539), CD8a-PE (1:200 dilution, Biolegend #162303), IFN γ -PE-Cy7 (1:100 dilution, Biolegend #505825), B220-BV605 (1:100 dilution, Biolegend #103243), NK1.1-APC (1:100 dilution, Biolegend #156505), F480-AF647 (1:100 dilution, BD Bioscience #565854), CD11b-PE-Cy7 (1:100 dilution, Biolegend #101215), CD11c-PE Dazzle 594 (1:100 dilution, Biolegend #117347) and MHCII-PerCp/Cy5.5 (1:100 dilution, Biolegend #103244). For IFN γ intracellular staining, we used an Intracellular Fixation and Permeabilization Buffer Set (eBioscience #88-8824-00, USA). The results were analyzed by FlowJo V10.5.3.

2.6. Total RNA extraction and RNA-sequencing analysis

Bone marrow cells were cultured from three individual wild-type mice or EphB1 knock-out mice, and BMDCs were cultured in complete RPMI supplemented with 20 ng/mL GM-CSF and 10 ng/mL IL-4 and were harvested using CD11c microbeads. Total RNA was isolated using a RNA Extraction Kit (Invitrogen #15596-026). RNA quality was assessed using Agilent 2100. All samples passed the quality assessment. RNA-sequencing were conducted based on the DNBSEQ platform, and analyses were conducted by R package DESeq2.

2.7. Western blot

Cell lysates were prepared using RIPA lysis buffer (BL504A, bio-sharp) containing 1 % PMSF and Phosphatase Inhibitor Cocktail (CWBIOT #CW2383, China). The total protein concentration was measured using the BCA Protein Quantification Kit (Vazyme #E112-01, China). Equal amounts of protein were separated by SDS-PAGE and transferred onto a 0.45 μ m PVDF membrane. The membranes were blocked in 5 % defatted milk in TBST and incubated overnight at 4 °C with diluted antibodies. The following primary antibodies were used: rabbit polyclonal anti-EphB1(y594) (1:1000 dilution, Abcam #ab61791, USA), rabbit polyclonal anti-COX2(1:1000 dilution, Affinity #AF7003, USA), rabbit polyclonal anti-beta actin (1:5000 dilution, Proteintech #81115-1-RR). After washing in TBST, the membrane was incubated with the secondary antibody HPR Goat Anti Rabbit (1:5000 dilution, Immunoway #RS0002, USA). The protein bands were visualized using the ECL Western Blotting Substrate (Millipore #WBULS0100, USA).

2.8. Data acquisition

The single-cell RNA sequencing (scRNA-seq) data (GSE131907,

GSE139555, GSE146100, GSE150660, and GSE176021) were obtained from Tumor Immune Single-cell Hub 2 (TISCH2, <http://tisch.comgenomics.org/home/>). The bulk tumor sequencing data from The Cancer Genome Atlas (TCGA), including RNA expression, DNA methylation, and copy number were collected from the UCSC Xena (<http://xena.ucsc.edu/>).

2.9. Single-cell data processing

The data were integrated using the R package ‘Harmony’ [21] and processed using the standard ‘Seurat’ method [22]. Cell annotation was identified according to TISCH2. Based on the enrichment of EphB1, dendritic cells (DC) were divided into different subgroups: EphB1-positive DC (EDC) and EphB1-negative DC (NEDC). Next, the regulation of transcription factors (TFs) was analyzed using the R package ‘SCENIC’ [23]. Gene function enrichment was performed using the R package ‘irGSEA’ available at <https://github.com/chuiqin/irGSEA>. The single-cell pseudotime trajectories were constructed with the R package ‘monocle3’ available at <https://github.com/cole-trapnell-lab/monocle3>.

2.10. Bulk-tissue data processing

To identify the proportion of different cells in bulk tumor samples, deconvolution analysis was conducted between the bulk-tissue and single-cell sequencing data using the R package ‘BisqueRNA’ [24]. The proportion difference between EphB1 EDC and EphB1 NEDC was calculated. Accordingly, cutoffs of 0.01 and -0.01 were set to divide LUAD into EphB1-EDC-enriched (EDCE) samples, middle samples, and EphB1-NEDC-enriched (NEDCE) samples. Then, seven types of cancer immune cycles [25] were evaluated to reflect the level of anticancer immune responses. Seventy-five immunomodulators [26] were examined for gene expression, DNA methylation, and copy number alteration.

2.11. Molecular docking and virtual screening

The three-dimensional structure was retrieved from the Protein Data Bank (<https://www.rcsb.org/structure/5MJA>). The crystal model (5MJA) was protonated and optimized by the MOE plugin “Quickprep”. The binding site of ligand 7O3 was set as the docking region. Protein and molecules structures were protonated under the AMBER10: EHT force field. The MOE plugin “Dock” was used to study the interaction between proteins and molecules. The induced fit docking protocol was used for molecular docking, in which the triangle match algorithm was used to generate the docking mode, London 8G was used as the scoring function to calculate the binding energy for each docking pose, and the top 100 docking poses were retained. Finally, these docking poses were further optimized under the induced fit algorithm using the GBVI/WAS 8G scoring function to calculate the binding affinity for the optimized docking poses. Based on the docking regions, the top five docking poses of the hemoglobin tetramer and compound were finally retained. The natural product library L6020, which is a collection of natural compounds or substances that are typically derived from natural sources such as plants, microorganisms, or marine organisms was used for compound selection. The properties including aqueous solubility, octanol/water partition coefficient, and human intestinal absorption, were analyzed using Stardrop software. The lead compound candidates were obtained from Topsience, China.

2.12. Statistical analysis

The statistical analysis was performed using the R software. The Wilcoxon test was used to identify differences between binary groups for continuous variables, and the Kruskal-Wallis’s test was employed among multiple groups. Fisher’s exact test was used to evaluate differences between groups for categorical variables. Additionally, survival analysis

was conducted using Kaplan-Meier curves with the log-rank test. Spearman correlation was used to assess correlation coefficients. All statistical tests were two-sided, and a *P*-value of less than 0.05 was considered statistically significant.

3. Results

3.1. Tumor formation in EphB1-deficient mice

To explore the implications of EphB1 in cancer progression, we generated EphB1 knockout (KO) mice on the C57BL/6 background. The strategy for generating EphB1^{-/-} mice is illustrated in Fig. 1A, where a targeting vector was introduced to disrupt the third exon of mouse

EphB1 genes. The genotypes of the EphB1 mice were determined using PCR (Fig. 1B). Both PCR and western blotting were used to evaluate the expression of EphB1 mutants (Fig. 1B and C). Furthermore, immunohistochemical staining of tissues confirmed the absence of EphB1 expression in EphB1^{-/-} mice (Supplementary Fig. 1A), thus validating the successful knockout of EphB1 at both the mRNA and protein levels. The EphB1^{-/-} mice displayed fertility and exhibited no observable external physical abnormalities or histological abnormalities (Supplementary Fig. 1B).

We established 2 types of tumor models: a subcutaneous syngeneic Lewis lung carcinoma (LLC) model and a patient-derived cell (PDC) xenograft model (Fig. 1D). In the subcutaneous LLC model, LLC cells were subcutaneously administered to both EphB1 WT and KO mice,

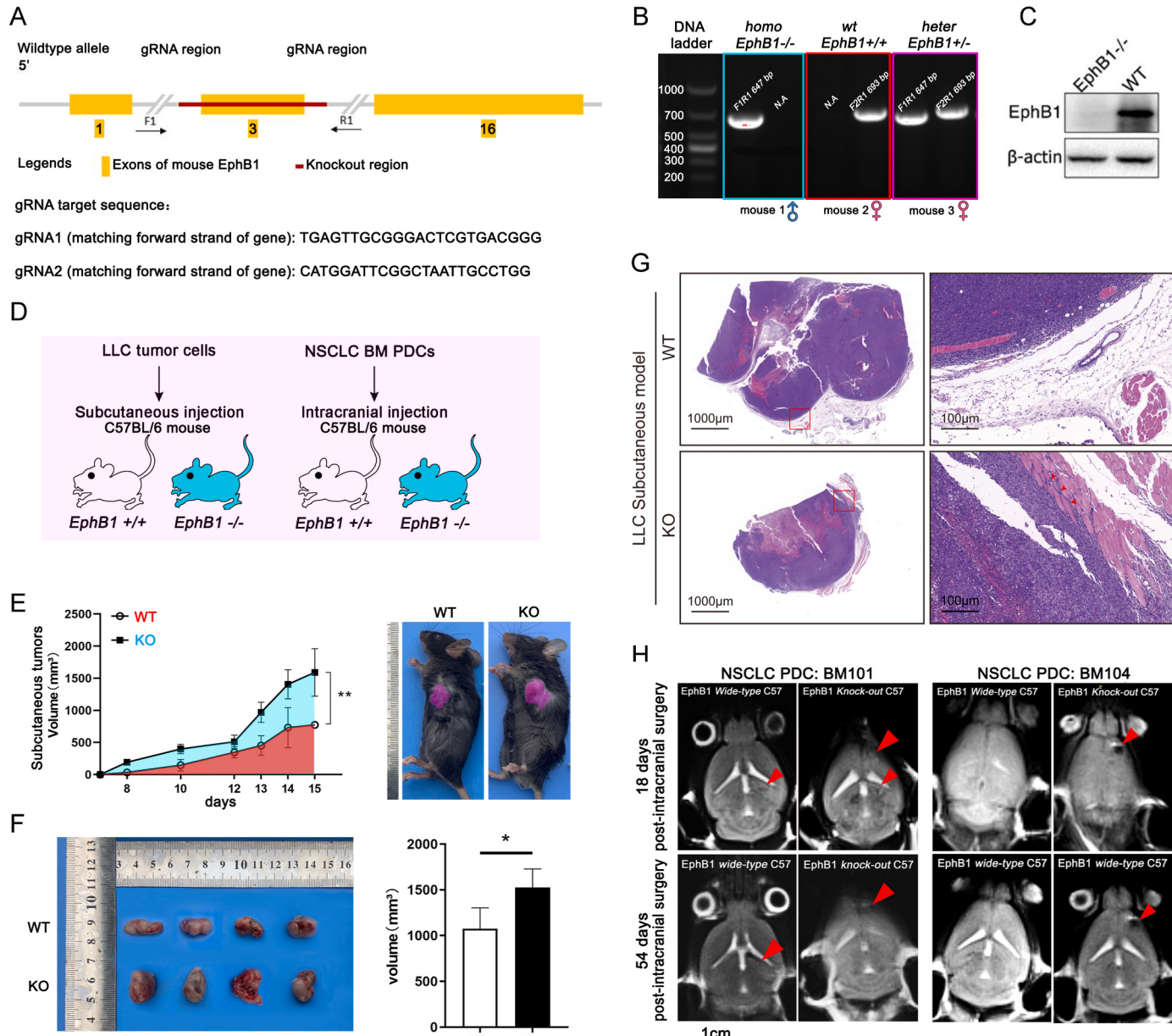


Fig. 1. Tumor formation in EphB1-deficient mice. EphB1 KO mice were generated on the C57BL/6 background. (A) The construct used to generate EphB1^{-/-} mice. A targeting vector disrupting the third exon of mouse EphB1 genes was introduced. The knockout of EphB1 was confirmed by RT-PCR (B) and western blot (C). F1R1 represents the targeted allele; N/A represents the negative control. (D) Two types of tumor models. The subcutaneous synergistic Lewis lung carcinoma (LLC) model and patient-derived tumor xenograft model were used to evaluate the cancer formation ability. (E) Tumor growth curve in LLC subcutaneously injected mice. ANOVA, ***P* < 0.01. (F) Tumors were excised, and the tumor volumes are shown on the right. (G) HE-stained cancer tissue sections. Arrows indicate the affected muscle fibers; (H)MRI images of the PDC xenograft model. Cancer cells from lung cancer brain metastases were intracranially injected into WT and KO mice. The formed tumors are indicated by red arrows.

resulting in tumor formation in all mice (Fig. 1E). Tumors exhibited accelerated growth in KO mice, and the size of tumors in KO mice was significantly larger than that of WT mice (Fig. 1E, 1F). Histological examination revealed that the tumors formed in KO mice exhibited a larger necrotic region, penetrating deeper into the muscle layer (Fig. 1G). Additionally, we observed splenic necrosis in KO mice, suggestive of inflammatory injury in the spleen (Supplementary Fig. 1C). Evaluation of CD45⁺ immune cells, including CD3⁺ T cells, CD11C⁺ MHCII⁺ DCs, B220⁺ B cells and CD11B⁺F480⁺ macrophages, demonstrated obvious reductions in T cells, DCs and macrophages in tumor-bearing KO mice (Supplementary Figs. 1D–1G). In the patient-derived cell xenograft model, cells obtained from lung cancer brain metastases were intracranially injected into both WT and KO mice (Fig. 1D). Magnetic resonance imaging was used to assess the intracranial growth of cancer cells. Similar to the LLC tumor model, PDCs formed larger tumors in KO mice than in their WT counterparts (Fig. 1H). Importantly, the PDC xenografts preserved the original phenotype observed in the patient, including the presence of a cavity in BM 104 (Fig. 1H). Our results indicate that the loss of EphB1 significantly promotes tumor formation *in vivo*.

3.2. EphB1-positive and -negative dendritic cells display distinct characteristics

We conducted an investigation to understand the immunological mechanisms underlying the association between EphB1 loss and increased tumor formation. We utilized publicly available single-cell RNA sequencing (scRNA-seq) datasets of lung cancer tissues (GSE 131907, GSE 139555, GSE146100, GSE 150660, GSE 176021) to examine the expression of EphB1 in immune cells. Our analysis encompassed a total of 1,115,184 cells from these 5 LUAD datasets (Supplementary Fig. 2A). Employing FlowSOM clustering and UMAP projection, we delineated the single-cell profiles into 16 clusters, with immune cells constituting the predominant cell types in cancer tissues (Fig. 2A). Marker genes and dataset sources for each cell subcluster are presented in Supplementary Fig. 2B. The cell type distribution in these datasets were shown in Supplementary Fig. 2C. Our analysis revealed that EphB1 expression predominantly resided in dendritic cells (DCs), epithelial cells and endothelial cells, with a particularly noteworthy presence in DCs (Fig. 2B). We then specifically examined the cell clusters designated as DCs and identified 26 subclusters of DCs (resolution = 0.8, Fig. 2C). Among these 26 subclusters of DCs, EphB1 emerged as the primary identifier in subcluster 13, which clearly distinguished two distinct DC populations (Fig. 2D). Accordingly, we identified 2 significant distinct DC types: EphB1-positive DCs (EDC, Cluster 13) and EphB1-negative DCs (NEDC, the other clusters) (Fig. 2E). EDCs exhibited elevated expression of GZMB, TSPAN13, PLD4, and others, while NEDCs displayed increased expression of ANXA5, CSTB, TIMP1, and others (Fig. 2E). To further investigate the association between these DCs and lung cancer progression, we assessed their abundance in primary tumors and tumors of different stages. EDCs were notably enriched in primary tumors and stage I tumors, whereas NEDCs predominated in metastatic tumors and advanced-stage tumors (Fig. 2F, G, 2H). These findings underscore EphB1's role in anticancer immunity.

We utilized SCENIC to examine the coexpression of transcription factors (TFs) and putative direct-binding targets. Our analysis revealed a regulatory distinction in transcription factor activity between the two groups. EphB1-positive DCs exhibited activated TFs such as UQCRB, BCL11A, RUNX2, NR3C1, and SPIB, while inhibited TFs included MAFB, SPI1, MAX extended, ETS2, and RAD21 extended (Fig. 2I). Additionally, we observed a significant downregulation of TNF- α signaling via NFkB, interferon- γ response, Interferon- α response, and apoptosis in the EphB1-positive DC group. In contrast, these signaling pathways were upregulated in the EphB1-negative DC group, which aligns with the observed inflammatory activation in KO mice (Fig. 2J). Pseudotime analysis indicated that EphB1-positive DCs formed a relatively independent subcluster separate from EphB1-negative DCs, with no

significant developmental transition between the two groups (Fig. 2K and 2L). To assess the expression level of EphB1 on DCs in the NSCLC dataset, we used the marker genes mentioned in Supplementary Fig. 2B to infer the cell proportions of each LUAD sample through a deconvolution method, using thresholds of 0.01 and –0.01 (Fig. 2M). Subsequently, we integrated LUAD transcriptomic sequencing data from the TCGA database using deconvolution methods. This classification led to the division of LUAD into three groups: EphB1-EDC-enriched (EDCE) samples, middle samples, and EphB1-NEDC-enriched (NEDCE) samples. Notably, patients with EDC-enriched samples exhibited longer survival than those with NEDC-enriched samples, providing compelling evidence of the potential anticancer effects of EDC (Fig. 2N).

3.3. EphB1 loss compromises the differentiation and maturation of dendritic cells

We then analyzed immune cells in WT and KO mice using flow cytometry. In EphB1^{−/−} mice, we observed similarities in B220⁺ B cells, NK1.1⁺ NK cells, DCs, and macrophage across peripheral blood, bone marrow, spleen and lungs when compared to WT mice. However, a noticeable reduction in the percentage of CD3⁺ T cells was observed in the spleens of EphB1^{−/−} mice compared with WT mice, suggesting a potential role of EphB1 in T-cell proliferation (Supplementary Figs. 3A–3E). Additionally, a significant decrease in the percentage of DCs (defined as CD45⁺/CD11C⁺/MHCII⁺) was evident in the brains of EphB1^{−/−} when mice compared to WT mice, indicating the presence of an immunosuppressive niche in the brains of EphB1^{−/−} mice (Fig. 3A).

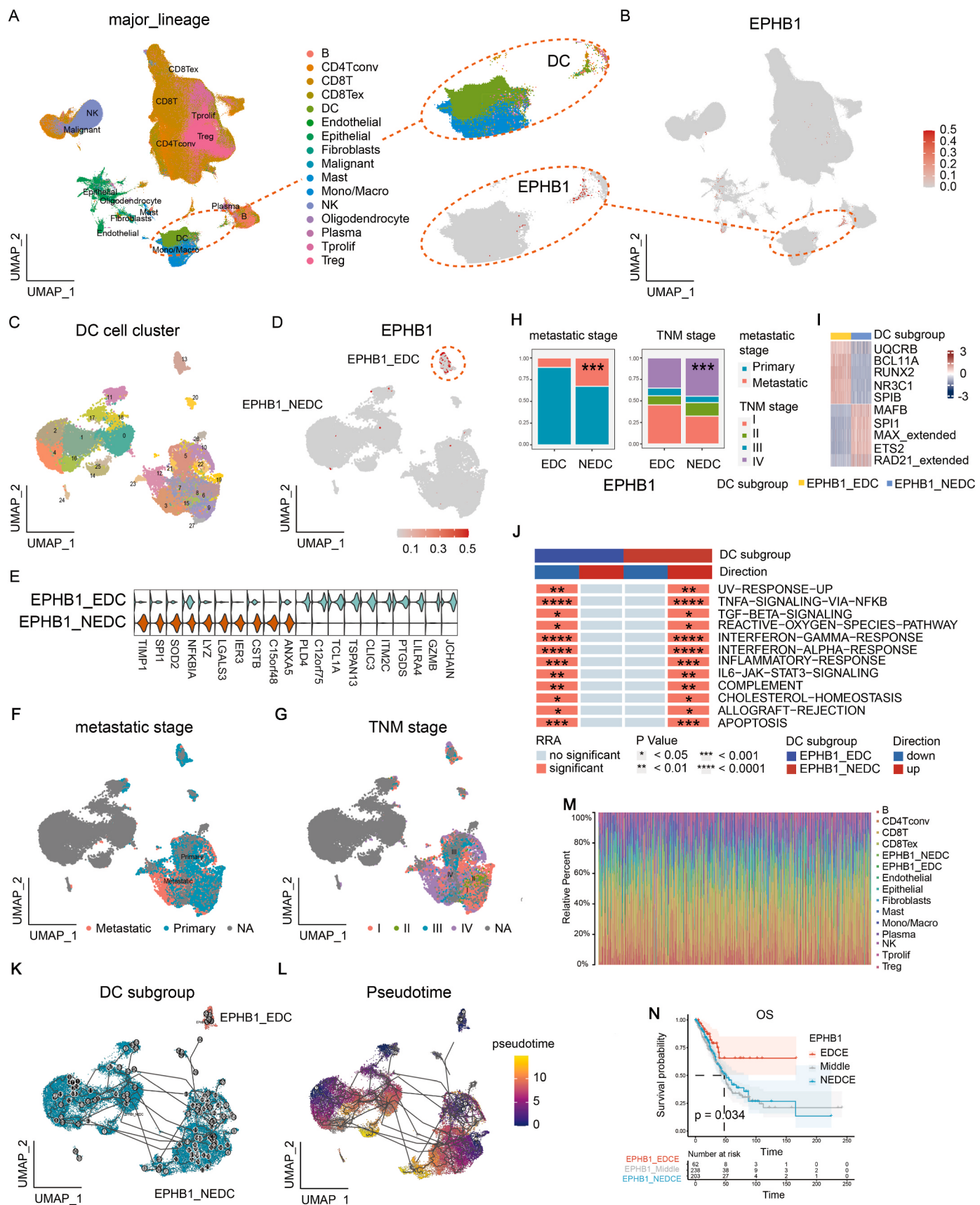
In our syngeneic subcutaneous tumor model, we observed a decreased number of CD11B⁺/CD11C⁺ DCs in the bone marrow, spleen and tumor of KO tumor-bearing mice compared to WT tumor-bearing mice (Fig. 3B, C, 3D). Similarly, a diminished number of CD11C⁺B220⁺ plasmacytoid dendritic cells (pDCs) was observed in the spleen and tumors in KO tumor-bearing mice compared to their WT counterparts (Fig. 3B, C, 3D). We also noted a reduction in CD8⁺IFN- γ ⁺ T cells in KO tumor-bearing mice, suggesting the involvement of EphB1 in cancer immunity (Fig. 3E). Furthermore, we identified colocalization of EphB1 and CD11C in tumor tissues from tumor-bearing mice or brain metastases from lung cancer patients (Fig. 3F, Supplementary Fig. 3F).

Furthermore, we observed a distinct decrease in CD11B⁺F480⁺ macrophages in the bone marrow and spleen of KO tumor-bearing mice compared to WT tumor-bearing mice. However, no substantial changes in macrophage populations within the tumors were observed (Supplementary Figs. 4A–4C). Based on our findings, we concluded that the loss of EphB1 impairs monocyte-to-macrophage and monocyte-to-DC differentiation.

3.4. EphB1 receptor tyrosine kinase mediates DC differentiation and maturation

We subsequently induced DC differentiation from the bone marrow of both KO and WT mice. Following induction with IL-4 and GM-CSF, we observed that KO DCs exhibited a reduced frequency of CD11B⁺CD11C⁺ immature DCs and CD11C⁺MHCII⁺ mature DCs compared to WT DCs (Fig. 4A). Upon treatment with LPS, the rates of CD11C⁺MHCII⁺ and CD11C⁺ CD86⁺ DCs were also lower in KO DCs than in WT DCs (Fig. 4B). These findings provide evidence that EphB1 plays a promotive role in DC differentiation and maturation.

Next, we treated mouse bone marrow cells with EphrinB2-FC, which activates EphB1 phosphorylation, and EphB1-FC, which inhibits EphB1 phosphorylation. As illustrated in Fig. 4C and D, EphrinB2-FC increased the population of CD11B⁺CD11C⁺ DCs, while EphB1-FC decreased their numbers. However, we did not observe any significant difference in the proportion of pDCs in the treated bone marrow cells. This suggests that EphB1 phosphorylation promotes DC differentiation and maturation.



(caption on next page)

Fig. 2. EphB1-positive and -negative dendritic cells display distinct characteristics. The expression of EphB1 in immune cells was analyzed in publicly accessible single-cell RNA-seq (scRNA seq) datasets of lung cancer tissues (GSE 131907, GSE 139555, GSE146100, GSE 150660, GSE 176021). (A) The cells were clustered using FlowSOM and visualized by UMAP projection. (B) EphB1 expression in dendritic cells (DCs), epithelial cells and endothelial cells, especially in DCs. (C) Subclusters of DCs. (D) The expression of EphB1 in subclusters of DCs. (E) Gene expression in EphB1-positive DCs (EDCs, Cluster 13) and EphB1-negative DCs (NEDCs, the other clusters); (F) (G) The distribution of EDCs and NEDCs in tumors with different clinical stages; (H)The distribution of EDCs and NEDCs in primary tumors and in metastatic tumors; (I) SCENIC analysis of the coexpression of transcription factors and putative direct-binding targets. “extended” refers to an expansion or enhancement of the analysis. (J) Signaling pathway activity in EDCs and NEDCs. (K) (L) EDCs and NEDCs; (M) Cellular proportions for LUAD samples obtained using the deconvolution method in the TCGA database; (N) Survival curve for patients with EDC compared to those with NEDC.

3.5. COX-2 is implicated in DC differentiation in EphB1 KO mice

To identify the factors involved in DC differentiation, we conducted an RNA-seq analysis comparing the transcriptomes of WT DCs and KO DCs. Total RNA was prepared from the IL-4- and GM-CSF-treated bone marrow cells of WT and KO mice. Principal component analysis (PCA) indicated a distinct separation based on gene expression between WT DCs and KO DCs (Fig. 5A). Among the genes, 119 genes were significantly upregulated and 44 genes were significantly downregulated in KO DCs compared to WT DCs ($|\log_2 \text{FC}| \geq 1$, $\text{Q value} \leq 0.05$, Fig. 5B). GO enrichment analyses demonstrated that the differentially expressed genes (DEGs) were associated with various signaling pathways, including the MAPK signaling pathway, NF κ B pathway and PI3K-Akt signaling (Fig. 5C). Notably, significantly highly expressed genes in KO DCs included PTGS2 (COX2), DUSP2, and IGF1 (Fig. 5D). Further analysis of single-cell sequencing data revealed significantly higher expression of COX2, MAPK14 and DUSP1 in EphB1-negative DCs (NEDC) than in EphB1-positive DCs (EDC, Fig. 5E). Subsequently, we focused on COX2, a key inflammatory enzyme. We treated bone marrow cells with Ephrin-B2 to activate EphB1 phosphorylation and with EphB1-fc to inhibit EphB1 phosphorylation. We found that EphB1 phosphorylation suppressed the expression of COX2 (Fig. 5F), suggesting that COX2 may be involved in the inflammatory response triggered by EphB1.

We then investigated the mechanisms by which EphB1 promotes the differentiation of DCs. Following treatment with IL-4 and GM-CSF, KO DCs exhibited upregulated PTGS2 (COX2). This increase in COX-2 expression in KO DCs was further confirmed through Western blot assay (Fig. 5G). Moreover, we observed that inhibiting COX-2 using celecoxib in naive bone marrow cells and IL-4- and GM-CSF-treated bone marrow cells led to enhanced expression of the cell surface molecules CD11C and MHCII (Fig. 5H and I). The reduced number of DCs in KO mice can be partly reversed by COX-2 inhibition (Fig. 5H and I), suggesting the involvement of COX-2 in DC differentiation in EphB1 KO mice.

3.6. TNP-000386 activates phosphorylation of EphB1 and inhibits tumor growth

To identify potential lead compounds for activating *p*-EphB1 and enhancing cancer immunity, we conducted a structure-based virtual screening of the natural product library L6020. EphB1 possesses a conserved intracellular tyrosine kinase domain, and we performed an in silico docking study targeting the pocket of the EphB1 kinase domain responsible for ATP binding (PDB ID:5MJA). Detailed results can be found in *Supplementary Table 1*. Among the candidates, we selected the top three lead compounds for further analysis: TANA-016837, TNP-000386 and TCD-04070014. We evaluated their binding affinity, energy scoring, Tanimoto scores, and binding mode toward the EphB1 kinase domain, revealing hydrophobic-hydrophobic interactions and a network of hydrogen bonds (Fig. 6A–F).

Our investigations revealed that TANA-016837, TNP-000386, and TCD-04070014 could induce the phosphorylation of EphB1 (Fig. 7A). Furthermore, treatment of bone marrow cells with these compounds significantly increased the population of CD11C $^+$ MHCII $^+$ DCs induced by IL-4 and GM-CSF, along with the populations of CD11C $^+$ CD80 $^+$ DCs and CD11C $^+$ CD86 $^+$ DCs. This suggests that these compounds promote

DC differentiation and maturation (Fig. 7B and C). As negative controls, we included demeclocycline, chlortetracycline and minocycline in our research, known as EphB1 kinase inhibitors [27]. Conversely, treatment of bone marrow cells with these control compounds significantly inhibited DC differentiation and maturation (Supplementary Fig. 5). These results underscore the influence of the lead compounds on DC differentiation and maturation through structure-based activation and inactivation of phosphorylated EphB1 signaling. As TNP-000386 exhibited the most potent effect among the 3 compounds, we proceeded to evaluate its efficacy using the C57/BL tumor mouse model. Subcutaneous injection of Lewis lung cancer (LLC) cells into C57BL/6 mice was performed, and when the tumors reached approximately 100 mm 3 , TNP-000386 was intraperitoneally injected into the tumor-bearing mice at a dose of approximately 50 mg/kg. As depicted in Fig. 7E, TNP-000386 significantly inhibited tumor growth (Fig. 7D and E). The immunofluorescence images confirmed the enhancing effect of TNP-000386 on EphB1 phosphorylation in both cancer cells and DCs (Fig. 7F).

4. Discussion

In this study, we have elucidated the pivotal role of EphB1 phosphorylation signaling in the differentiation and maturation of DCs. To harness its tumor-suppressive effects and influence the DC immune response to inhibit tumor growth *in vivo*, we employed lead compounds guided by the EphB1 phosphorylation region. Additionally, we discovered that phosphorylated EphB1 can downregulate COX-2 expression, thereby enhancing DC functions.

EphB1, a receptor tyrosine kinase, is a central player in various cellular processes, including cell migration, adhesion, and differentiation. Its activity, especially phosphorylation, which occurs at specific tyrosine residues within the protein, is known to impact immune cells such as DCs, T cells and natural killer cells [11]. The phosphorylation of EphB1 has been shown to regulate T-cell activation, proliferation, and cytokine production [15]. Dysregulation of EphB1 phosphorylation has been linked to various diseases, including cancer, neurodegenerative disorders, and cardiovascular diseases [3,27,28].

Despite EphB1 overexpression in tumor tissues, accumulating evidence suggests a dual and often contradictory role for EphB1 in cancer. Phosphorylation-induced activation of EphB1 has been linked to its ability to impede tumor growth, invasion, and metastasis [29,30]. In this study, we demonstrate that phosphorylation of EphB1 is a crucial factor in DC differentiation and maturation, highlighting the potential of EphB1 phosphorylation as a therapeutic target to harness its tumor-suppressive effects. EphB1 signaling has been implicated in the regulation of proinflammatory cytokine production in immune cells, such as TNF- α and IL-6 [31]. In addition, EphB1 is known to play a role in leukocyte migration and adhesion, processes crucial to the inflammatory response [32]. Dysregulation of EphB1 signaling has been associated with the development of inflammatory diseases, such as rheumatoid arthritis and multiple sclerosis [33]. In rheumatoid arthritis, EphB1 has been found to be overexpressed in synovial tissue and promotes the production of proinflammatory cytokines by synovial fibroblasts. In experimental models of multiple sclerosis, EphB1 is involved in the migration of immune cells into the central nervous system, contributing to the development of the disease [32]. However, recent research has shown that EphB1 has anti-inflammatory effects in

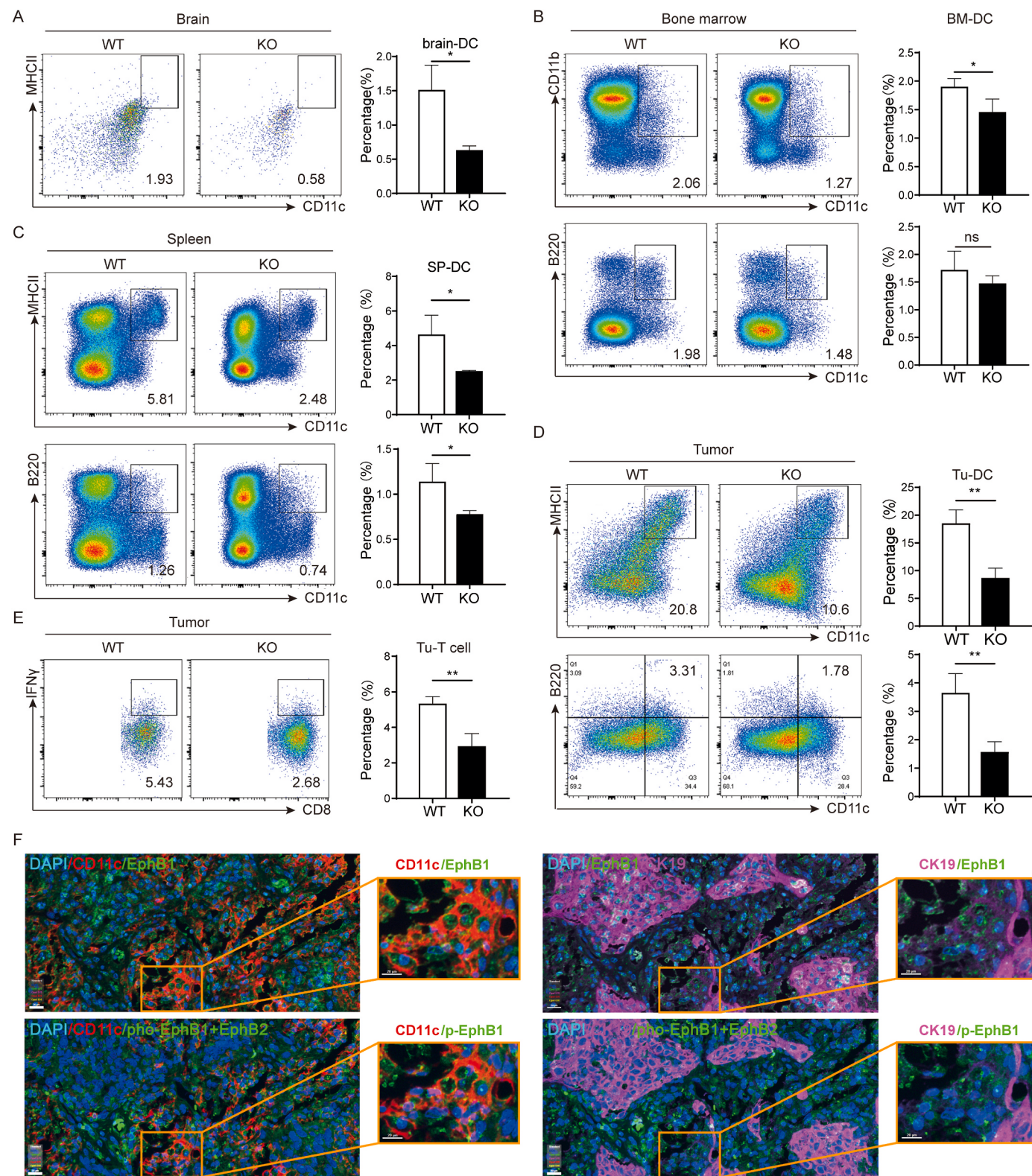


Fig. 3. EphB1 loss compromises the differentiation and maturation of dendritic cells. (A) The percentage of DCs (defined as $CD45^+$, $CD11C^+$, $MHCII^+$) in the brains of $EphB1^{-/-}$ mice was measured by flow cytometry. The percentage of $CD11B^+$ $CD11C^+$ cDCs and $B220^+$ $CD11C^+$ pDCs in bone marrow (B), spleen (C) and tumor (D) in tumor-bearing WT and KO mice was measured by flow cytometry. ($N = 3$) (E) The percentage of $CD8^+$ $IFN-\gamma^+$ T cells in tumor-bearing mice in WT and KO mice. ($N = 3$) Student's T test, * $P < 0.05$, ** $P < 0.01$, NS: no significance. (F) The immunofluorescence images of EphB1 and CD11C in tumor tissues from tumor-bearing mice. The positive cells are indicated by arrows.

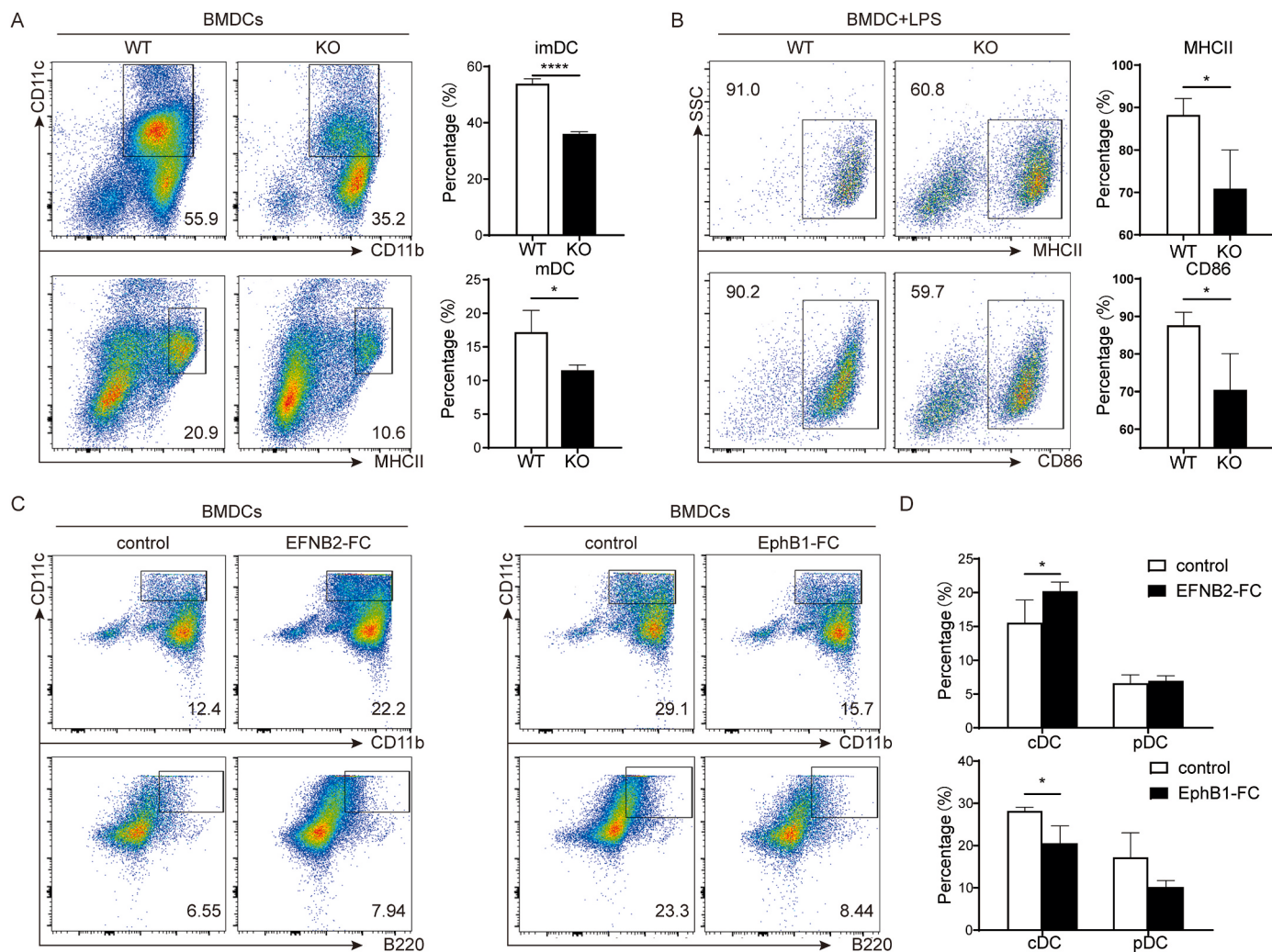


Fig. 4. EphB1 receptor tyrosine kinase mediates DC differentiation and maturation. (A) The percentage of immature DCs (defined as CD45⁺, CD11C⁺, CD11b⁺) and mature DCs (defined as CD45⁺, CD11C⁺, MHCII⁺) in bone marrow cells from EphB1 WT and KO mice was measured by flow cytometry. (N = 3) (B) The percentage of CD11C⁺MHCII⁺ and CD11C⁺CD86⁺ DCs after treatment with LPS in bone marrow cells from EphB1 WT and KO mice. (N = 3) (C) The percentage of CD11C⁺CD11b⁺ cDCs and CD11C⁺B220⁺ pDCs in bone marrow cells after treatment with EphB1-FC and EphB1-FC. (D) The flow cytometry results are shown in the column chart. Student's T test, *P < 0.05 (N = 3).

astrocytes, partially through STAT3 [34]. It has long been accepted that PGE2, a product of COX-2, suppresses the cell-mediated immune response by inhibiting IL-2 and IFN- γ and enhancing IL-10 [35]. PGE2 stimulates COX-2 expression via MAPK p38 but not ERK in DC-like cells [36]. These findings underscore the complex role of EphB1 in inflammation, encompassing both pro- and anti-inflammatory effects. In this study, we reveal that phosphorylated EphB1 promotes DC function partly through inhibiting the expression of COX-2, a key enzyme involved in the production of proinflammatory molecules.

Computational approaches have become indispensable in drug discovery, particularly during the early stages of drug development. One of their key applications is the docking of small molecules into the pocket structure of target proteins, enabling virtual screening to identify potential drug candidates [37]. Docking involves the prediction of the binding affinity between a small molecule and a target protein by analyzing the structural features using molecular modeling techniques such as molecular dynamics simulations, quantum mechanics/molecular mechanics calculations, and scoring functions. Docking simulations estimate the binding energy between small molecules and targets, helping to identify promising compounds [38]. Ligand- or structure-based virtual screening is the main virtual screening method [38]. In this study, we utilized docking and scoring in virtual screening

to identify compounds that act as stimulants for EphB1 phosphorylation. We selected 3 compounds with the highest scores and confirmed their stimulating effect on EphB1 phosphorylation. However, it is important to note that computational approaches have their limitations. Factors such as the quality of the target protein structure, the scoring function used, and the conformational flexibility of the ligand and protein can affect the accuracy of docking simulations. Therefore, it is crucial to confirm computational results through experimental assays such as binding and cell-based assays.

The study of EphB1 phosphorylation has yielded valuable insights into the regulation of immune cell function and holds promise for informing the development of new therapeutic approaches across various diseases. However, further studies are needed to elucidate the underlying mechanisms and determine whether targeting EphB1 signaling could be a viable therapeutic approach for inflammatory diseases.

5. Conclusion

Our findings demonstrate impaired differentiation of DCs in EphB1^{-/-} mice, whereas the activation of EphB1 phosphorylation stimulates DC differentiation and maturation. Furthermore, we identified lead

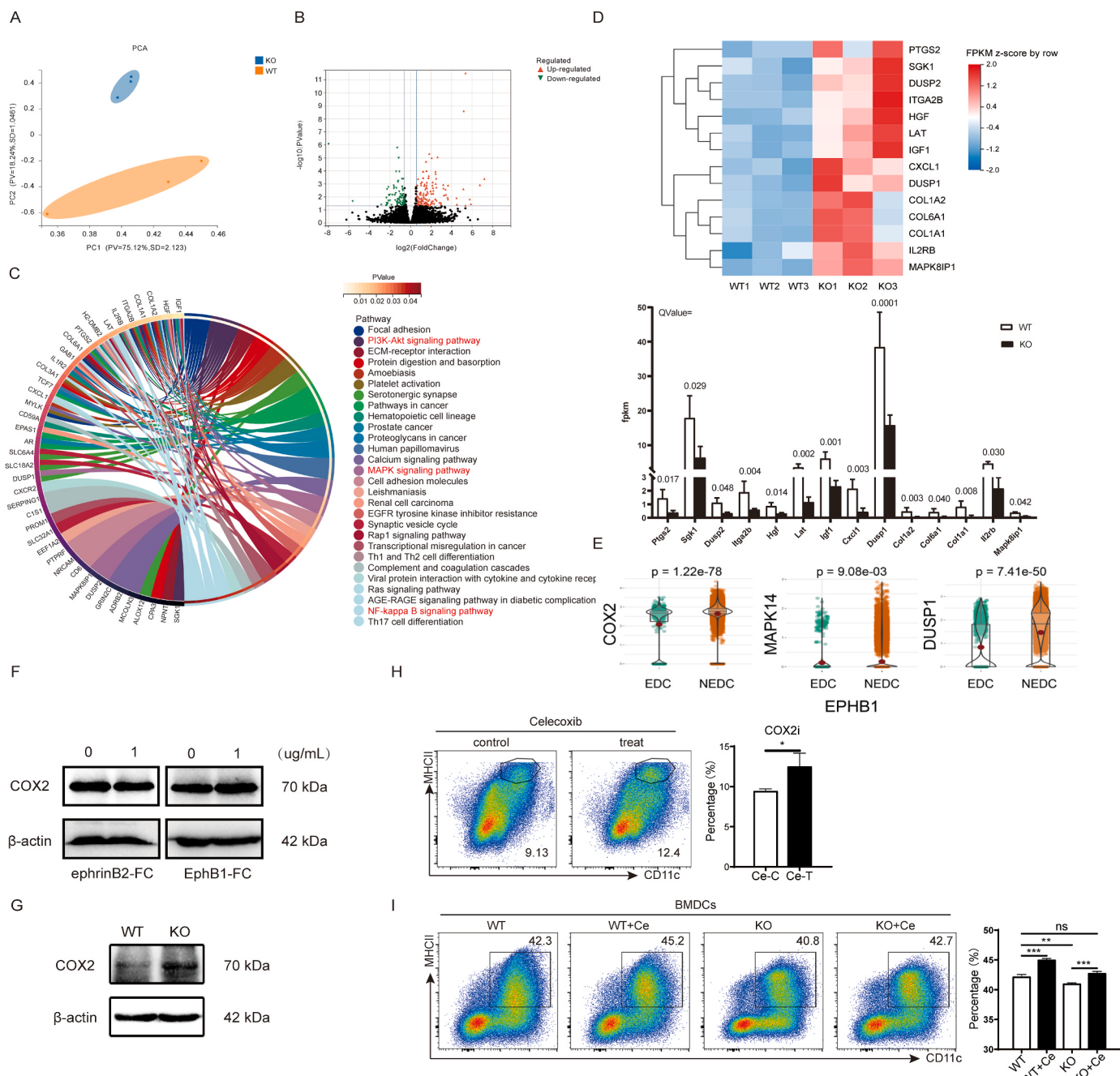


Fig. 5. COX-2 is implicated in DC differentiation in EphB1 KO mice. Bone marrow cells from EphB1 WT and KO mice were subjected to RNA-seq following treatment with IL-4 and GM-CSF. (A) PCA analysis. (B) The DEGs are shown in the volcano plot. (C) GO analyses of DEGs; (D) Heatmap of DEGs (above) and histogram showing the expression levels of key genes (below). The numbers indicate the q values. (E) The expression of COX2, MAPK14 and DUSP1 in EphB1-negative DCs (NEDC) compared to EphB1-positive DCs (EDC) was analyzed in publicly accessible single-cell RNA-seq (scRNA seq) datasets of lung cancer tissues (GSE 131907, GSE 139555, GSE146100, GSE 150660, GSE 176021). (F) The expression of COX2 measured by Western blot after treatment with ephrinB2-FC and EphB1-FC. (G) Cox-2 expression in KO DCs. The percentage of CD11C⁺MHCII⁺ DCs in naive bone marrow cells (H) and IL-4- and GM-CSF-treated bone marrow cells (I) after treatment with the COX-2 inhibitor celecoxib. (N = 3) Student's T test, *P < 0.05, **P < 0.01, ***P < 0.001. DEGs: differentially expressed genes.

compounds that target the phosphorylation sites 602–896 of EphB1 and verified their enhancing effects on cancer immunity.

Funds

This work was supported by National Natural Science Foundation, China (grant number 81773147, 81972198); Natural Science Foundation of Hunan Province (grant number 2023JJ30972, 2023JJ40853); Natural Science Foundation, Changsha (grant number: kq2208299,

kq2208337); Strategic Priority Research Program of Central South University (ZLXD2017004); Health Special Fund Research Project of Hunan province (B2021-04).

Data availability statement

The single-cell RNA sequencing (scRNA-seq) data were acquired from the Tumor Immune Single-cell Hub 2 (TISCH2) repository, accessible at <http://tisch.comp-genomics.org/home/>. The specific datasets

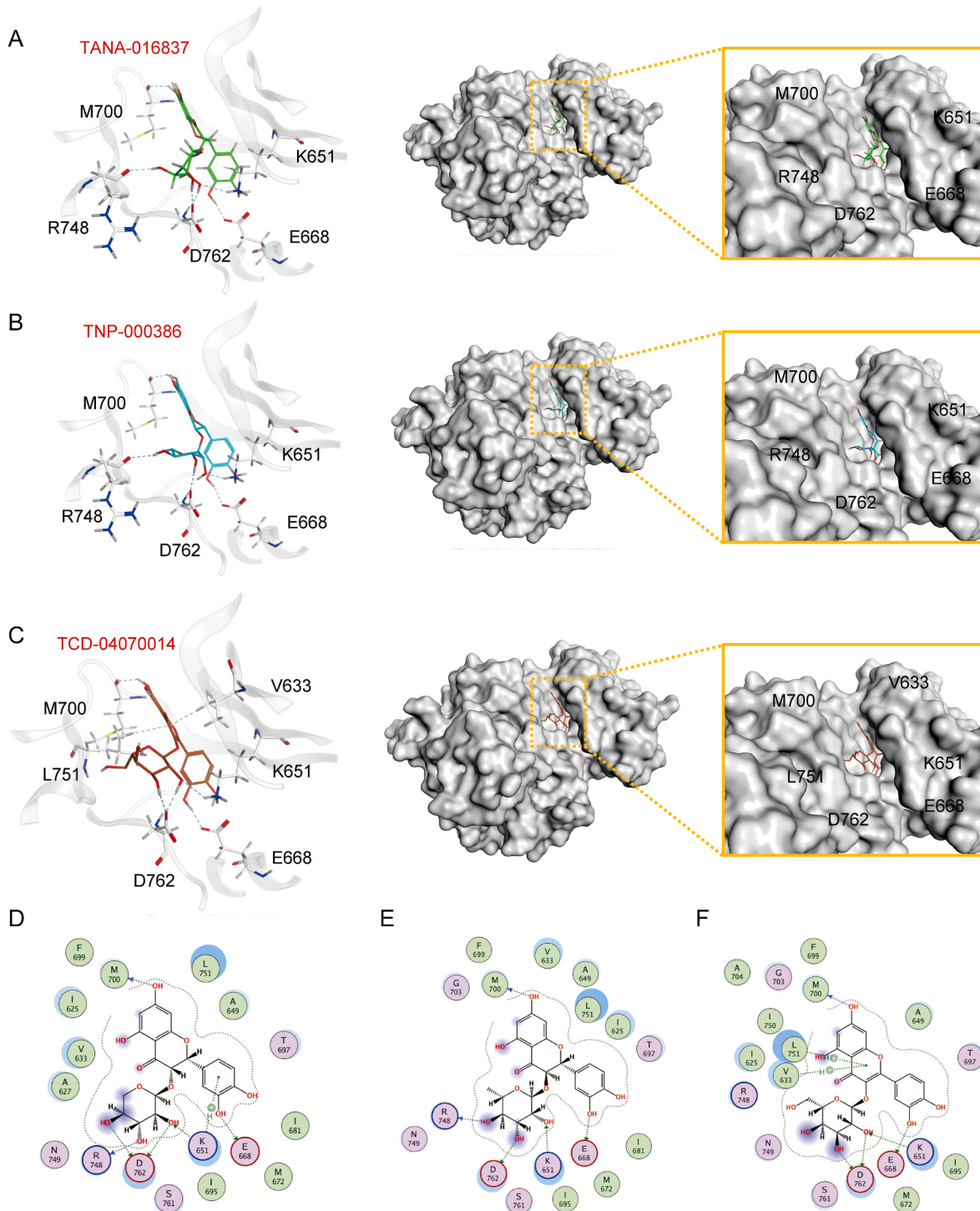


Fig. 6. Binding models of lead compounds with EphB1. (A) TANA-016837; (B) TNP-000386; (C) TCD-04070014 binding mode with EphB1. Left: Surface map of the binding mode, where the white surface represents the protein surface of EphB1 and the green carbon stick model represents these screened compounds; Right: 3D model of the binding mode, where the white cartoon represents EphB1 protein, the blue dashed line represents hydrogen bonds, and the green dashed line represents hydrogen-aromatic ring interactions; 2D model of the binding mode for (D)TANA-016837; (E) TNP-000386; (F)TCD-04070014, where the green and blue arrows represent hydrogen bonds, and the green H and dashed lines represent hydrogen-aromatic ring interactions with the benzene ring. Structural analysis of the EphB1 kinase domain (619–882 site) is indicated with a yellow cycle.

utilized in this study include GSE131907, GSE139555, GSE146100, GSE150660, and GSE176021.

To complement the single-cell data, bulk tumor sequencing data from The Cancer Genome Atlas (TCGA) were collected. The TCGA bulk tumor data were accessed through the UCSC Xena platform, available at <http://xena.ucsc.edu/>.

Declaration of generative AI in scientific writing

The authors declare that we only use the AI-assisted technologies to improve readability and we carefully review and edit the language of the work.

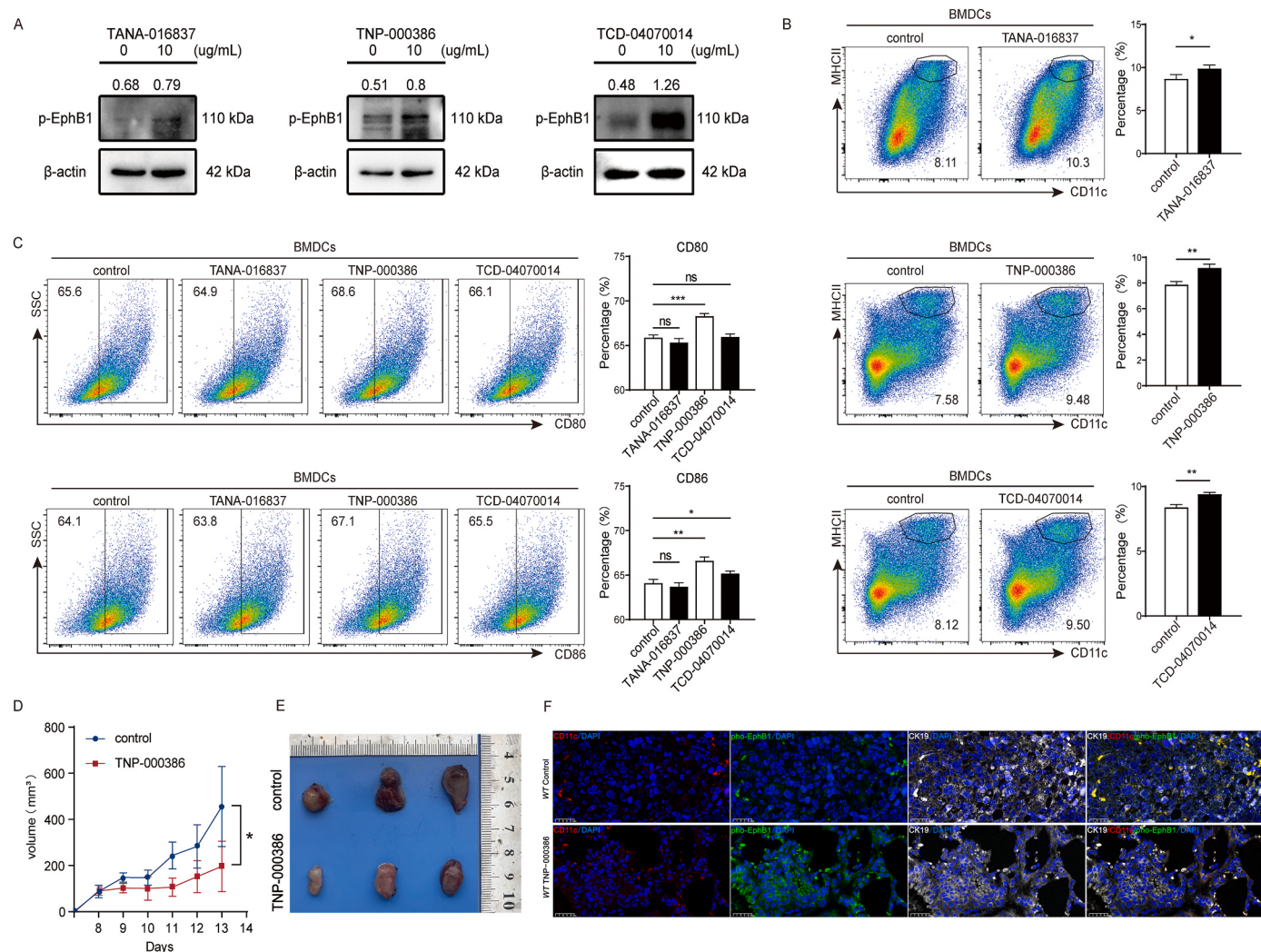


Fig. 7. TNP-000386 activates phosphorylation of EphB1 and inhibits tumor growth. An in silico docking study along with the pocket of the EphB1 kinase domain for ATP binding (PDB code:5MJA) was performed. The top three lead compounds were selected and tested for activation potency, including TANA-016837, TNP-000386 and TCD-04070014. (A) The phosphorylation of EphB1 activated by TANA-016837, TNP-000386 and TCD-04070014 was evaluated by western blot. The number above bands indicates the gray values for p-EphB1 bands normalized to the β-actin bands. (B) The percentage of CD11c⁺MHCII⁺ DCs in IL-4- and GM-CSF-induced bone marrow cells after treatment with TANA-016837, TNP-000386 and TCD-04070014. (N = 3) (C) The percentage of CD11c⁺CD80⁺ and CD11c⁺CD86⁺ mature DCs in LPS-induced bone marrow cells after treatment with TANA-016837, TNP-000386 and TCD-04070014. (N = 3); The Lewis lung cancer (LLC) cells were subcutaneously injected into C57BL/6 mice. When the tumors reached approximately 100 mm³, TNP-000386 was intraperitoneally injected into tumor-bearing mice at approximately 50 mg/kg (D) Growth curve of tumor-bearing mice; (E) Excised tumor samples; (F) The immunofluorescence images of EphB1 phosphorylation in both cancer cells and DCs.

CRediT authorship contribution statement

Yaohuan Xie: Writing – original draft, Visualization, Software, Methodology, Formal analysis, Data curation. **Liyang Zhang:** Validation, Software, Methodology, Funding acquisition, Formal analysis, Data curation. **Lujuan Wang:** Methodology, Data curation, Conceptualization. **Bo Chen:** Software, Methodology, Data curation. **Xiaoting Guo:** Software, Methodology, Data curation. **Yanyi Yang:** Validation, Visualization. **Wenhua Shi:** Visualization, Software, Methodology, Data curation. **Anqi Chen:** Software, Methodology, Data curation. **Junqi Yi:** Software, Methodology, Data curation. **Jingqun Tang:** Validation, Supervision, Project administration, Investigation, Conceptualization. **Juanjuan Xiang:** Writing – review & editing, Supervision, Project administration, Methodology, Investigation, Funding acquisition, Formal analysis, Conceptualization.

Declaration of competing interest

We declare that we have no competing financial interests or personal relationships that could influence the work reported in this paper.

Acknowledgements

I am deeply thankful for the support and assistance provided by Yue Ning, who is working as a pathologist in the second Xiangya Hospital, Central South University.

Appendix A. Supplementary data

Supplementary data to this article can be found online at <https://doi.org/10.1016/j.canlet.2023.216567>.

References

- [1] E.M. Lisabeth, G. Falivelli, E.B. Pasquale, Eph receptor signaling and ephrins, *Cold Spring Harbor Perspect. Biol.* 5 (9) (2013).
- [2] L.Y. Liang, et al., Eph receptor signalling: from catalytic to non-catalytic functions, *Oncogene* 38 (39) (2019) 6567–6584.
- [3] L. Wang, et al., Cell-cell contact-driven EphB1 cis- and trans- signalings regulate cancer stem cells enrichment after chemotherapy, *Cell Death Dis.* 13 (11) (2022) 980.
- [4] D. Arvanitis, A. Davy, Eph/ephrin signaling: networks, *Genes Dev.* 22 (4) (2008) 416–429.
- [5] A. Cecchini, D.D.W. Cornelison, Eph/ephrin-based protein complexes: the importance of cis interactions in guiding cellular processes, *Front. Mol. Biosci.* 8 (2021), 809364.
- [6] I. Dudanova, R. Klein, The axon's balancing act: cis- and trans-interactions between Ephs and ephrins, *Neuron* 71 (1) (2011) 1–3.
- [7] S.M. Shamah, et al., EphA receptors regulate growth cone dynamics through the novel guanine nucleotide exchange factor ephexin, *Cell* 105 (2) (2001) 233–244.
- [8] S. Bhatia, et al., Knockdown of EphB1 receptor decreases medulloblastoma cell growth and migration and increases cellular radiosensitization, *Oncotarget* 6 (11) (2015) 8929–8946.
- [9] W. Wei, H. Wang, S. Ji, Paradoxes of the EphB1 receptor in malignant brain tumors, *Cancer Cell Int.* 17 (2017) 21.
- [10] L. Wang, et al., Ligand-independent EphB1 signaling mediates TGF-beta-activated CDH2 and promotes lung cancer cell invasion and migration, *J. Cancer* 11 (14) (2020) 4123–4131.
- [11] E. Shiuan, J. Chen, Eph receptor tyrosine kinases in tumor immunity, *Cancer Res.* 76 (22) (2016) 6452–6457.
- [12] S. Yamaguchi, et al., Immunotherapy of murine colon cancer using receptor tyrosine kinase EphA2-derived peptide-pulsed dendritic cell vaccines, *Cancer* 110 (7) (2007) 1469–1477.
- [13] M. Hatano, et al., Vaccination with EphA2-derived T cell-epitopes promotes immunity against both EphA2-expressing and EphA2-negative tumors, *J. Transl. Med.* 2 (1) (2004) 40.
- [14] M. Li, et al., Treatment of Dutch rat models of glioma using EphrinA1-PE38/GM-CSF chitosan nanoparticles by in situ activation of dendritic cells, *Tumour Biol.* 36 (10) (2015) 7961–7966.
- [15] T.K. Darling, T.J. Lamb, Emerging roles for Eph receptors and ephrin ligands in immunity, *Front. Immunol.* 10 (2019) 1473.
- [16] M.C. Rissoan, et al., Subtractive hybridization reveals the expression of immunoglobulin-like transcript 7, Eph-B1, granzyme B, and 3 novel transcripts in human plasmacytoid dendritic cells, *Blood* 100 (9) (2002) 3295–3303.
- [17] G. Yu, et al., Ephrin-B1 is critical in T-cell development, *J. Biol. Chem.* 281 (15) (2006) 10222–10229.
- [18] T.M. Nguyen, et al., EphB and Ephrin-B interactions mediate human mesenchymal stem cell suppression of activated T-cells, *Stem Cell. Dev.* 22 (20) (2013) 2751–2764.
- [19] H. Kawano, et al., A novel feedback mechanism by Ephrin-B1/B2 in T-cell activation involves a concentration-dependent switch from costimulation to inhibition, *Eur. J. Immunol.* 42 (6) (2012) 1562–1572.
- [20] L. Zhang, et al., A novel integrated system using patient-derived glioma cerebral organoids and xenografts for disease modeling and drug screening, *Cancer Lett.* 500 (2021) 87–97.
- [21] I. Korsunsky, et al., Fast, sensitive and accurate integration of single-cell data with Harmony, *Nat. Methods* 16 (12) (2019) 1289–1296.
- [22] R. Satija, et al., Spatial reconstruction of single-cell gene expression data, *Nat. Biotechnol.* 33 (5) (2015) 495–502.
- [23] S. Aibar, et al., SCENIC: single-cell regulatory network inference and clustering, *Nat. Methods* 14 (11) (2017) 1083–1086.
- [24] B. Jew, et al., Accurate estimation of cell composition in bulk expression through robust integration of single-cell information, *Nat. Commun.* 11 (1) (2020) 1971.
- [25] L. Xu, et al., TIP: a web server for resolving tumor immunophenotype profiling, *Cancer Res.* 78 (23) (2018) 6575–6580.
- [26] T.X. Huang, L. Fu, The immune landscape of esophageal cancer, *Cancer Commun.* 39 (1) (2019) 79.
- [27] M.J. Chumley, et al., EphB receptors regulate stem/progenitor cell proliferation, migration, and polarity during hippocampal neurogenesis, *J. Neurosci.* 27 (49) (2007) 13481–13490.
- [28] C. Tiruppathi, et al., EphB1 interaction with caveolin-1 in endothelial cells modulates caveolae biogenesis, *Mol. Biol. Cell* 31 (11) (2020) 1167–1182.
- [29] H. Davies, et al., Somatic mutations of the protein kinase gene family in human lung cancer, *Cancer Res.* 65 (17) (2005) 7591–7595.
- [30] H. Alazzouzi, et al., Mechanisms of inactivation of the receptor tyrosine kinase EPHB2 in colorectal tumors, *Cancer Res.* 65 (22) (2005) 10170–10173.
- [31] S.T. Liu, et al., EphrinB/EphB forward signaling in Muller cells causes apoptosis of retinal ganglion cells by increasing tumor necrosis factor alpha production in rat experimental glaucomatous model, *Acta Neuropathol. Commun.* 6 (1) (2018) 111.
- [32] T. Kitamura, et al., Enhancement of lymphocyte migration and cytokine production by ephrinB1 system in rheumatoid arthritis, *Am. J. Physiol. Cell Physiol.* 294 (1) (2008) C189–C196.
- [33] M.G. Coulthard, et al., Eph/Ephrin signaling in injury and inflammation, *Am. J. Pathol.* 181 (5) (2012) 1493–1503.
- [34] G.E. Tyzack, et al., A neuroprotective astrocyte state is induced by neuronal signal EphB1 but fails in ALS models, *Nat. Commun.* 8 (1) (2017) 1164.
- [35] F.G. Snijderswint, et al., Prostaglandin E2 differentially modulates cytokine secretion profiles of human T helper lymphocytes, *J. Immunol.* 150 (12) (1993) 5321–5329.
- [36] W. Cho, J. Choe, Prostaglandin E2 stimulates COX-2 expression via mitogen-activated protein kinase p38 but not ERK in human follicular dendritic cell-like cells, *BMC Immunol.* 21 (1) (2020) 20.
- [37] X.Y. Meng, et al., Molecular docking: a powerful approach for structure-based drug discovery, *Curr. Comput. Aided Drug Des.* 7 (2) (2011) 146–157.
- [38] D.B. Kitchen, et al., Docking and scoring in virtual screening for drug discovery: methods and applications, *Nat. Rev. Drug Discov.* 3 (11) (2004) 935–949.